Geotechnical Engineering
Volume 167 Issue GE4

Three-dimensional analysis of a concrete-face rockfill dam
Mahabad, Imam, Javanmardi and Jalali

ice | proceedings

Proceedings of the Institution of Civil Engineers
Geotechnical Engineering 167 August 2014 Issue GE4
Pages 323–343 http://dx.doi.org/10.1680/geng.11.00027
Paper 1100027
Received 05/03/2011 Accepted 02/03/2012
Published online 03/09/2012
Keywords: dams, barrages & reservoirs/slabs & plates/stress analysis/embankments

ice Institution of Civil Engineers publishing

Three-dimensional analysis of a concrete-face rockfill dam

1 **Nariman Mahabadi Mahabad** MSc
Student of hydraulic structures, Amirkabir University of Technology, Tehran, Iran

2 **Reza Imam** PhD
Assistant Professor, Amirkabir University of Technology, Tehran

3 **Yousef Javanmardi**
PhD student of geotechnical engineering, Amirkabir University of Technology, Tehran, Iran

4 **Hossein Jalali** PhD
Head, Ab-Nirou Consulting Engineering Company, Tehran, Iran




The behaviour of a proposed concrete-face rockfill dam and its face slab during first impounding are examined using three-dimensional finite-element modelling, verified by results of empirical relationships and observed behaviour of similar dams. The study is carried out on the Glevard dam, a 110 m high concrete-face rockfill dam with a crest length of 276 m. Two models are used for the face slab, one with vertical joints and one without. Friction contacts are used between the concrete face and the underlying rockfill, and between adjacent slab pieces, such that relative sliding at these contacts is allowed. Slab deformations and stresses, joint openings and axial forces obtained for the two models are compared. Results indicate that while neglecting face slab joints in the analysis may not significantly influence the calculated total deformations, it can result in substantial underestimation of in-plane horizontal deformations and axial forces, especially near the abutments. In-plane deformations influence the performance of water stops and leakage through slab joints, and axial forces influence slab design. Results also show that using relatively simple geometry and material modelling in a three-dimensional finite-element analysis can yield results in reasonably good agreement with the observed behaviour and the empirical relations obtained from similar dams.

Notation

A CFRD upstream slope face area
C cohesion
D maximum deformation of CFRD face slab after first impounding
E Young's modulus
E_v vertical deformation modulus of CFRD
H dam height
L crest length
U total deformation of dam body
γ unit weight
ν Poisson's ratio
ϕ friction angle of cushion material

1. Introduction

1.1 CFRDs and their advantages

Concrete-face rockfill dams (CFRDs) are known to have originated from the mining regions of Sierra Nevada in California in the 1850s; however, construction of modern dams started only in the late 1960s and early 1970s. Since then, rapid progress has been achieved in the construction of CFRDs throughout the world. This is due mainly to the distinct advantages in the economy, efficiency and performance of these dams, such that several CFRDs more than 200 m high have been successfully designed and constructed throughout the world so far. Some advantages of CFRDs are listed below in terms of their material, construction and performance.

(*a*) Material: rockfill is a cost-effective construction material and a good energy dissipater, as observed during partial fillings in extreme floods before the concrete face was built. Rockfill has been observed to be able to accept high leakage safely: therefore diversion capacity can be reduced by allowing overtopping of the rockfill.
(*b*) Construction: rockfill is suitable for wet weather placement; foundation grouting can be done in parallel with rockfill placement; multistage construction of the rockfill embankment is possible; foundation clean-up requires no hard work except at the plinth; and the plinth and face slab can be constructed quickly and economically using slip forming.
(*c*) Performance: water load is transferred to the foundation upstream of the dam axis, resulting in increased stability and a high factor of safety against sliding; post-construction

movements are often small, and stop only several years after construction; the dam performs well during earthquake owing to the dry rockfill and the lack of pore pressures; and little or no instrumentation is required for monitoring dam safety.

Construction of CFRDs involves placing well-compacted, higher-grade rock in the dam core and/or upstream slope, and lower-grade and/or less-compacted rock in the downstream slope areas. The use of better compaction or material in the upstream slope is intended to result in a better support for, and less deflection of, the concrete face slab, which is usually constructed after the upstream slope is placed. The face slab is supported at its bottom edge by a plinth, which is a reinforced concrete section constructed along the toe of the upstream slope. The plinth may be anchored to the dam foundation in order to provide sufficient support for the lateral loads transferred from the face slab. A grout curtain may also be constructed under the plinth to control seepage and reduce possible erosion of the foundation. A perimeter joint is constructed where the face slab meets the plinth, in order to allow for their relative displacements or deformations.

1.2 Performance of CFRDs

Many aspects of the design and performance of CFRDs and rockfill dams have been studied. Compilations of measured data on construction settlements and face slab deformations (Pinto and Marques, 1998), deformations during earthquakes (Swaisgood, 1995), seepage through foundations (Giesecke *et al.*, 1991), leakage rates through the dam body (ICOLD, 2004) and other aspects of CFRD behaviour have been presented, and empirical prediction methods for dam performance based on these databases have been developed. Details of the design, construction and performance of CFRDs are also provided in several publications (e.g. Hunter *et al.*, 2003; ICOLD, 2004).

The concrete face slab of a CFRD is its main water barrier. It also transfers water pressure to the rockfill and finally to the foundation. In the design of CFRDs, special attention should therefore be paid to the behaviour of the face slab, particularly during impounding, since it is often constructed after rockfill placement, and most engineering problems arise from dam deformations, leakage caused by joint damages and breakage of the face slab following impounding.

Giudici *et al.* (2000) studied the behaviour of face slabs based on observations obtained from instrumented CFRDs in Australia. They showed that the water pressure applied on the face slab during impounding exerts loads with horizontal and vertical components on the upstream slope, with the horizontal component causing it to deform towards the downstream, and the vertical component resulting in its settlement. The face slab deformations follow those of the upstream slope: therefore proper selection and compaction of the upstream slope rockfill material are of primary importance. These deformations lead to in-plane movements of the face slab towards its centre and away from the abutments, causing it to remain in compression over most of its area and in extension near the dam abutments.

Since the role of the face slab as the main water barrier for the dam depends mainly on its overall behaviour and movements rather than on its strength, its thickness and reinforcement have often been selected based on precedent. However, recent case histories have indicated that this can lead to excessive face deformations, slab cracking and high rates of seepage (ICOLD, 2004). Analysis of the dam and its face slab should therefore be carried out, taking into account the actual valley geometry, the dam material properties, and the shape, properties and details of the face slab.

Pinto and Marques (1998) developed a database of various measured behaviour parameters and construction conditions of some CFRDs, and derived relationships for the estimation of dam behaviour parameters, including maximum face slab deformation during impounding. Table 1 presents some data obtained from their database.

1.3 Objectives of the current study

Because of the complex mechanisms affecting the behaviour of CFRD face slabs, including their interaction with the underlying rockfill, the effects of valley shape, and construction details, there is a need to consider 3D effects for the study of first reservoir filling, especially in narrow valleys. Comprehensive studies involving 3D numerical analyses of CFRDs during first impounding are rare, and, in particular, the need to model the performance of vertical joints at the face slabs has not been sufficiently justified (Marulanda and Anthiniac, 2009).

The current research involves three-dimensional (3D) finite-element (FE) analysis of the Glevard Neka dam, a 110 m high CFRD with a crest length of 276 m, which is currently under construction by the Ev-Yol–Abniru joint venture on the Nekarud River in northern Iran. The purpose of this study is to predict the behaviour of this dam and its concrete face slab during first impounding. Previous studies (e.g. Noorzaei and Mohammadian, 2000) have shown that the behaviour of CFRDs can be predicted reasonably well if appropriate numerical modelling and material properties are used.

Since vertical joints play an important role in the behaviour of face slabs of CFRDs during first impounding (Kashiwayanagi *et al.*, 2000), two models were considered in the analysis: one with vertical joints (model A) and the other without (model B). In CFRDs, the use and location of vertical joints depend on the construction procedures, and on whether adjacent slab sections are expected to move relative to each other under reservoir operation.

The current study involves face slab behaviour during first impounding; because of a lack of creep data on the dam material, it does not address long-term creep deformations of the rockfill

Dam	Country	Year	Height: m	L: m	A: 10^3 m^2	A/H^2	E: MPa	D: cm	Joint opening: mm	Leakage: l/s
Cethana	Australia	1971	110	213	24	2·0	135	12	11·5	7
Anchicayá	Colombia	1974	140	260	22	1·1	145	13	125	1800/800[a]
Fox do Areia	Brazil	1980	160	828	139	5·4	32	69	23	236/60
Segredo	Brazil	1993	140	705	86	4·4	45	34	–	400/50
Xingo	Brazil	1994	140	850	135	6·9	37	30	30	180
Aguamilpa	Mexico	1993	187	660	137	3·9	190	<15	19	260/100
Salvajina	Colombia	1984	148	330	50	2·3	390	<10	7	60
Golillas	Colombia	1984	130	125	14	0·9	210	16	–	1080/650
Shiroro	Nigeria	1984	125	560	65	4·2	76	–	30	1800/100
Lower Pieman	Australia	1986	122	–	35	2·4	160	22	7	–
Machintosh	Australia	1981	75	–	27	4·8	40	16	4·8	14
Murchison	Australia	1982	89	–	16	2·0	225	4	12	2
Bastyan	Australia	1983	75	–	19	3·4	160	6	4·8	7
Khao Laem	Thailand	1984	130	1000	140	8·3	45	13	5	53
Kotmale	Sri Lanka	1984	97	620	60	6·4	50	–	2	–

L = crest length.
D = deformation of face slab, measured at mid-height, with full reservoir
[a]Initial leakage/value after repair works.

Table 1. Specifications and performance parameters of some CFRDs (data from Pinto and Marques, 1998)

material, or their possible effects on the face slab behaviour. Hunter *et al.* (2003) indicate that for well-compacted medium- to high-strength rockfill, long-term crest settlement resulting from creep ranges from 0·05% to 0·25% of dam height for each log cycle of time. This results in about a 10–50% increase in settlements, and their associated other deformations, for each log cycle of time after construction of the face slab.

1.4 The Glevard Neka dam

Figure 1 shows the layout of the Glevard dam, and Table 2 presents some of its geometrical properties. Details regarding the zoning of the dam cross-section are provided in Section 2.2 and in Figure 6.

Construction work for the dam started in February 2010. Placing and compacting of rockfill for the dam body commenced in June 2011, and is planned to be completed by August 2012, with about 30% of its volume completed as of November 2011. The dam body consists of three zones: the upstream slope, the middle zone and the downstream slope. The maximum sizes of rockfill for these zones are 0·6 m, 0·8 m and 1·2 m and placement layer thicknesses are 1 m, 1·2 m and 1·5 m respectively. The use of middle-size rockfill in the middle section is intended to prevent sudden changes in rock size and the development of cracks due to such changes. Good-quality rockfill is used for the upstream slope zone, quarry rockfill for the downstream slope zone, and

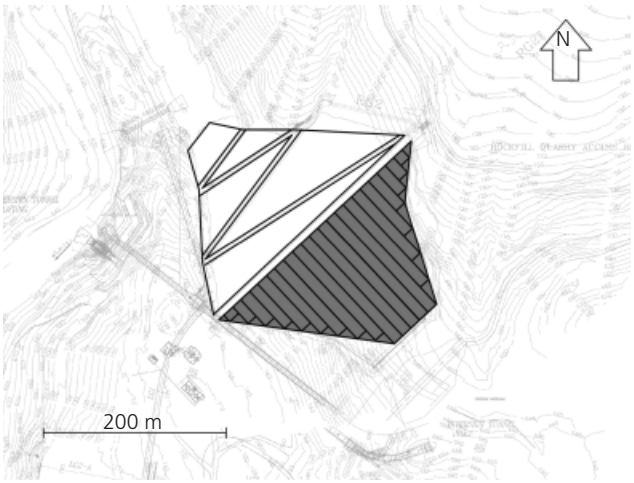

Figure 1. Layout of Glevard Neka CFRD

lower-quality quarry run for the middle zone. Each layer is compacted by specified passes of heavy vibrating rollers to achieve the required compaction.

Construction of the concrete face slab is planned to start in September 2012, one month after completion of the dam main body, and end in July 2013. The slab will have vertical joints, and

Dimension	Value
Dam height from bed: m	110
Crest length: m	275
Crest width: m	10
Foundation thickness: m	100
Foundation length: m	600 (perpendicular to dam axis)
Foundation width: m	475 (along dam axis)
Minimum thickness of concrete face: cm	40 at dam crest (El. 739 amsl)
Maximum thickness of concrete face: cm	80 at upstream toe (El. 629 amsl)
Upstream slope, H:V	1·45:1
Downstream slope, H:V	1·35:1

Table 2. Dimensions of 3D FE model of Glevard dam

its construction will start with building a starter slab, followed by constructing odd-numbered slab panels and joint water stops, and then even-numbered panels. A cushion layer underneath the face slab, and a transition zone underneath the cushion layer and above the upstream slope rockfill material of the main dam body, will also be constructed. The cushion layer and transition zone will each be 4–5 m thick, and will consist of material with maximum grain sizes of 80 mm and 200 mm respectively. Dam crest construction will then start and will last for four months, ending in November 2013. Finally, dam impoundment is planned to commence in December 2013.

Instrumentation is planned to be installed to monitor the behaviour of both the dam body and the face slab. It includes electric piezometers inside the upstream cushion layer to monitor leakage through the concrete face, Casagrande piezometers at low elevations in the downstream slope to monitor the downstream water level, and piezometers inside observation wells at the upstream slopes, near the concrete face, to monitor groundwater elevations. Biaxial vertical and horizontal inclinometers will be installed in the dam body to monitor its horizontal and vertical movements. Inclined inclinometers with capabilities for measuring horizontal and vertical movements are also planned to be installed at the face slab/cushion layer interface to monitor movements of the face slab following impoundment. Instrumentation of the face slab is designed to monitor the following three main items.

(*a*) Horizontal and vertical movements of the slab due to impoundment, and during normal dam operation.
(*b*) Movements of the slab joints, including the perimeter joint. These are monitored using 3D and one-dimensional (1D) joint meters installed at the slab and perimeter joints.
(*c*) Leakage at the slab joints or water level at the cushion layer. Leakage at the face slab–plinth connection and along the perimeter joint is also determined using a distributed fibre optic cable system that is capable of measuring seepage.

In addition, other instrumentation is also planned to be installed, such as accelerographs at the dam crest, rock extensometers in the rock foundation under the plinth and a V-notch weir at the dam downstream slope.

2. Modelling of the dam

2.1 Finite-element modelling of the dam

Based on the dam dimensions, the geometrical properties of the 3D FE model used for the analysis of the Glevard dam are shown in Table 2.

In evaluating the behaviour of the concrete face slab, two models were considered: model A, in which the face slab consists of 23 slabs separated by vertical joints 12 m apart; and model B, in which the face slab consists of a single slab without vertical joints. Both models are shown in Figure 2. Interface (interaction) elements were used at the rockfill/slab interface, as shown in Figure 3, and between adjacent face slabs, as shown in Figure 4. These elements provide a frictional-type contact, which allows the face slabs to slide on the underlying rockfill, and relative to each other.

Except for the face slab features, models A and B were the same in their foundation and rockfill details. The dam body and foundation were modelled using tetrahedral elements, with sizes varying from 6 m for the dam body to 50 m for the outer surfaces

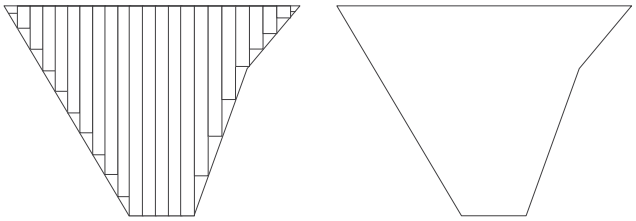

Figure 2. Model A (left, slab with vertical joints) and model B (right, single slab)

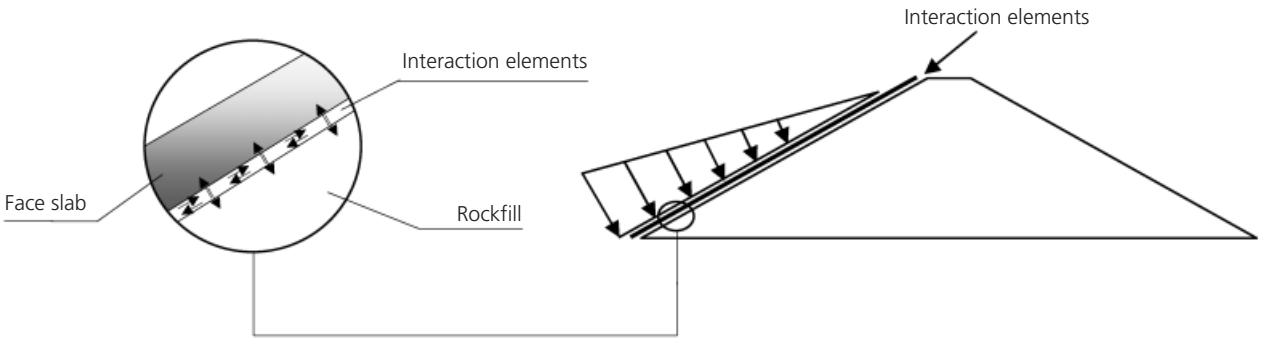

Figure 3. Interaction elements between face slabs and underlying rockfill for models A and B

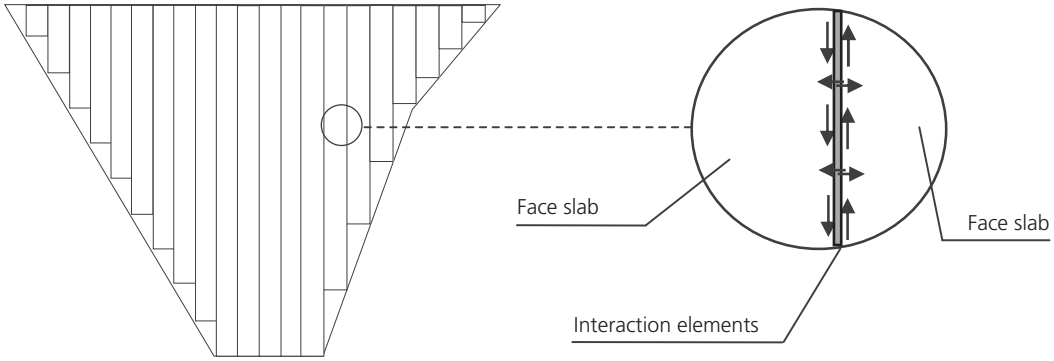

Figure 4. Interaction elements between adjacent face slabs for model A

of the dam foundation. The face slab was modelled using triangular shell elements 6 m in size, such that they are compatible with the mesh size used for the underlying dam body. These element sizes were chosen after some sensitivity analyses were performed to obtain the most efficient FE mesh for the 3D analysis. In this respect, in areas where high variations of stresses and deformations occur over small distances, element sizes were sufficiently small to enable accurate determination of these variations. An efficient combination of small elements at the dam body and dam/foundation interface, and larger elements at the foundation away from the dam/foundation interface was used, as shown in Figure 5. The total number of elements used for the foundation and dam body was 46 268, and the number of nodes was 10 291.

2.2 Material modelling

The main purpose of the current study is to examine the behaviour of the concrete face slab, which is constructed after placing the rockfill material, under the impounding load. However, in order to describe the selection of material properties for the current analysis, a brief explanation of the procedure used for the determination of end of construction displacements is also provided here.

Figure 6 shows the material types and zoning, and Table 3 shows the material properties used in the FE modelling of the construction of the Glevard dam. Construction stages were modelled by consecutively applying layers of rockfill material, with the number of layers being 40 at the highest (maximum) section and less at the shorter sections. In situ properties of the foundation and abutments were obtained using results of in situ pressure meter and standard penetration tests, complemented by triaxial and unconfined compression tests on samples recovered during site investigations. The properties of the rockfill were estimated using correlations between the specifications from the Glevard dam material and databases of properties of similar materials (e.g. ICOLD, 2004; Pinto and Marques, 1998), taking into account the stress dependence of the friction angle of the rockfill. A linear elastic stress–strain relationship and a Mohr–Coulomb failure criterion using the material properties shown in Table 3 were used for a 3D FE analysis, and these results were then compared with results obtained from 2D FE analyses from three transverse sections of the dam, in which the non-linear elastic (Duncan Chang) model was used for the rockfill material. Good agreement between the results of the 2D and 3D analyses was obtained, and therefore the linear elastic model with the Mohr–Coulomb failure criterion was used in the 3D analysis in order to save on

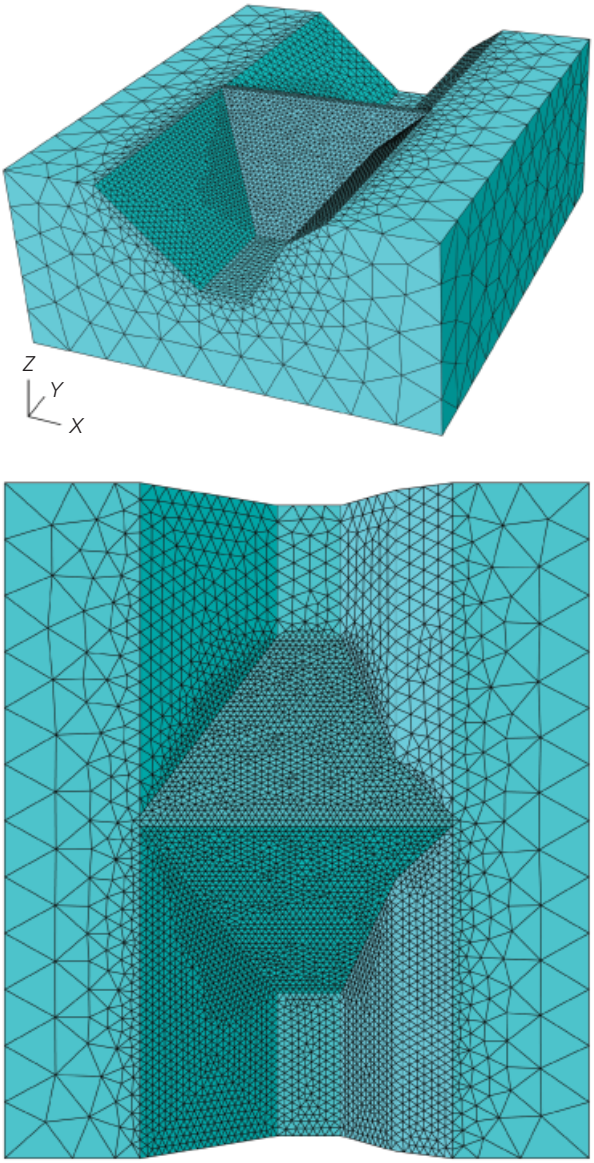

Figure 5. 3D FE model of dam body and foundation

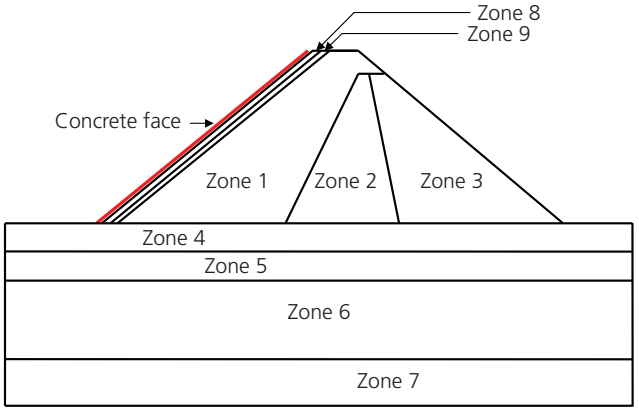

Figure 6. Geometry and zoning of 3D FE model used for Glevard CFRD

computational effort. Details of these analyses and the material parameters used for the 2D and 3D modelling are described by Ev Yol–Ab Niru (2010a, 2010b).

Based on the results described above, and because of the relatively small deformations usually experienced by CFRDs constructed with reasonably competent materials, as observed in databases of actual dam deformations (e.g. Pinto and Marques, 1998), the linear elastic model was considered suitable for the 3D modelling of the Glevard dam. In the case of the 110 m high Glevard dam, the maximum construction settlement was computed at about mid-height of the highest (maximum) section, and was only 0·57 m (Ev Yol–Ab Niru, 2010b). This value is about 0·5% of the dam height, and the approximately parabolic variations of settlement with elevation obtained from the 3D FE analysis were found to be closely consistent with the settlements observed in CFRDs with similar geometry and material properties, and with results obtained from empirical relationships derived from observed settlements of rockfill dams (ICOLD, 2004).

Zone no.	Zone description/formation name	Poisson's ratio, ν	γ (dry): kN/m^3	γ (sat): kN/m^3	C: kPa	ϕ: degrees	E: MPa
1	Upstream rockfill	0·25	19	20	0	51	100
2	Middle rockfill	0·25	19	20	0	45	100
3	Downstream rockfill	0·25	19	20	0	51	100
4	Laar	0·19	26	26·5	670	24	2100
5	Upper Shemshak	0·28	24	24·5	520	29	2700
6	Shemshak	0·26	24	25	540	21	1800
7	Gorgan	0·25	23	24	360	16	600
8	Cushion	0·25	19	20	0	33	100
9	Transition	0·25	19	20	0	45	100

Table 3. Material properties used in 3D FE modelling of construction of Glevard dam

Considering the material zoning and properties shown in Table 3, and the explanations provided above, the dam body and foundation were modelled using the material properties shown in Table 4 in order to simplify the analysis without losing much accuracy. A linear elastic stress–strain relationship and a Mohr–Coulomb failure criterion were used for modelling the dam body, foundation and face slab materials. The friction contacts used between the face slab and upstream rockfill, and between adjacent pieces of the face slab, simulate the condition of simple tensionless contact, with the hydrostatic load providing the normal forces to resist sliding between the slab and the underlying rockfill. Considering the properties of the cushion layer placed underneath the concrete face slab, a friction coefficient of 0·65 was used for the stiffness of the interaction elements. This value was obtained by applying a two-thirds reduction factor to $\tan\phi$ in which ϕ is the friction angle of the cushion material, estimated at about 45°. The friction coefficient between adjacent slab pieces is expected to have a small effect on the results of the analyses, since, as shown later, owing to the load of impounding, slab pieces tend to separate from each other.

3. Results of analyses

3.1 Dam body deformations due to impounding

Contours of total deformations obtained from the 3D analyses of the Glevard dam body during first impounding for models A and B are shown in Figure 7. These deformations are those experienced by the face slab due to first reservoir filling. The maximum calculated total deformation for model A is 24·8 cm for the dam body and 25·1 cm for the face slab, as will be shown later. For model B, the maximum total deformations of the dam body and face slab are 24·6 cm and 24·8 cm respectively. The total deformations of the upstream slope and face slab are the resultants of three components: a vertical component (upstream slope settlement), a horizontal component perpendicular to the dam axis (movement towards downstream) and a horizontal in-plane component along the dam axis.

3.2 Face slab deformations

Figure 8 shows contours of calculated total deformations, and Figures 9 and 10 show contours of horizontal deformations perpendicular to and along the dam axis respectively, due to impounding. For both models A and B, total deformations and horizontal deformations perpendicular to the dam axis are similar, and their maximum values are about 25 cm and 16 cm respectively, in both models. The overall pattern of deformations indicates that, owing to the load of impounding, the face slab both settles and moves horizontally towards the downstream, with the maximum values of these deformations occurring approximately in the dam mid-section.

However, unlike the total deformations and the horizontal deformations perpendicular to the dam axis, the horizontal in-plane deformations vary somewhat differently in models A and B, with their maximum values being approximately 3·9 cm and 2·5 cm for these models respectively. Although the horizontal in-plane deformations are substantially smaller than those perpendicular to the dam axis, they can have a greater influence on the separation of the slab pieces, the performance of the water stops and the potential seepage at the slab joints in model A. Comparison of Figures 8, 9 and 10 shows that whereas the other deformations vary almost continuously across adjacent slab joints in model A, the horizontal in-plane deformations vary discontinuously, indicating that some separation of adjacent slab pieces is taking place at the joint locations. The overall pattern of these deformations is such that sections of the slab on the two sides deform towards the middle section, those on the right abutment deform towards the left, and those on the left abutment deform towards the right. This is a result of the highest downward and downstream deformations occurring in the mid-section of the slab, as discussed before, such that parts of the slab on the sides are pulled towards the middle.

The accuracy of the results obtained from the FE analysis were verified by comparing them with those obtained from the empirical relationship presented by Pinto and Marques (1998). This relationship is derived from measurements of actual CFRD face-slab deformations during impounding. According to this relationship, the maximum face slab deformation is proportional to the ratio H^2/E_v, in which H is the dam height in metres and E_v is the vertical deformation modulus of the rockfill in MPa. The ratio of proportionality increases with the valley shape factor A/H^2, in which A is the upstream slope face area in m^2. A shape factor smaller than 3 is an indication of a narrow valley (ICOLD, 2004). For the Glevard dam, the valley shape factor is about 2·4, and the corresponding proportionality ratio is 0·14. Therefore the following relationship applies for this dam

$$D = 0{\cdot}14\frac{H^2}{E_v} \quad (1)$$

Zone	E: MPa	Poisson's ratio, ν	γ: kN/m^3	C: kPa	ϕ: degrees	Material model
Rockfill	100	0·25	19	0	51	Mohr–Coulomb
Foundation	1900	0·25	26	550	25	Mohr–Coulomb
Face slab	25 000	0·17	25	–	–	Linear elastic

Table 4. Material properties used in 3D analysis of behaviour of concrete face slab

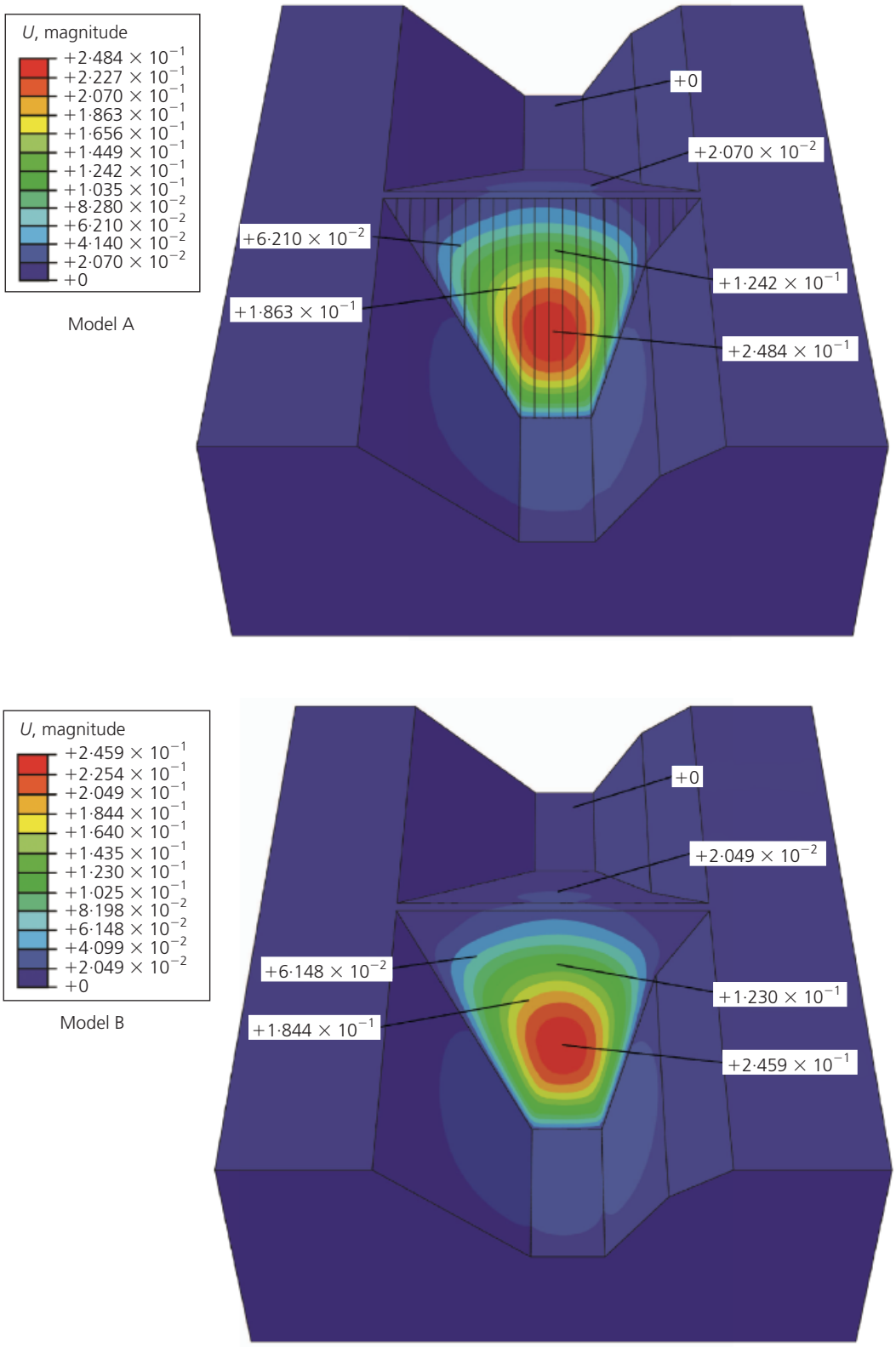

Figure 7. Comparison between total deformations of dam body for models A and B

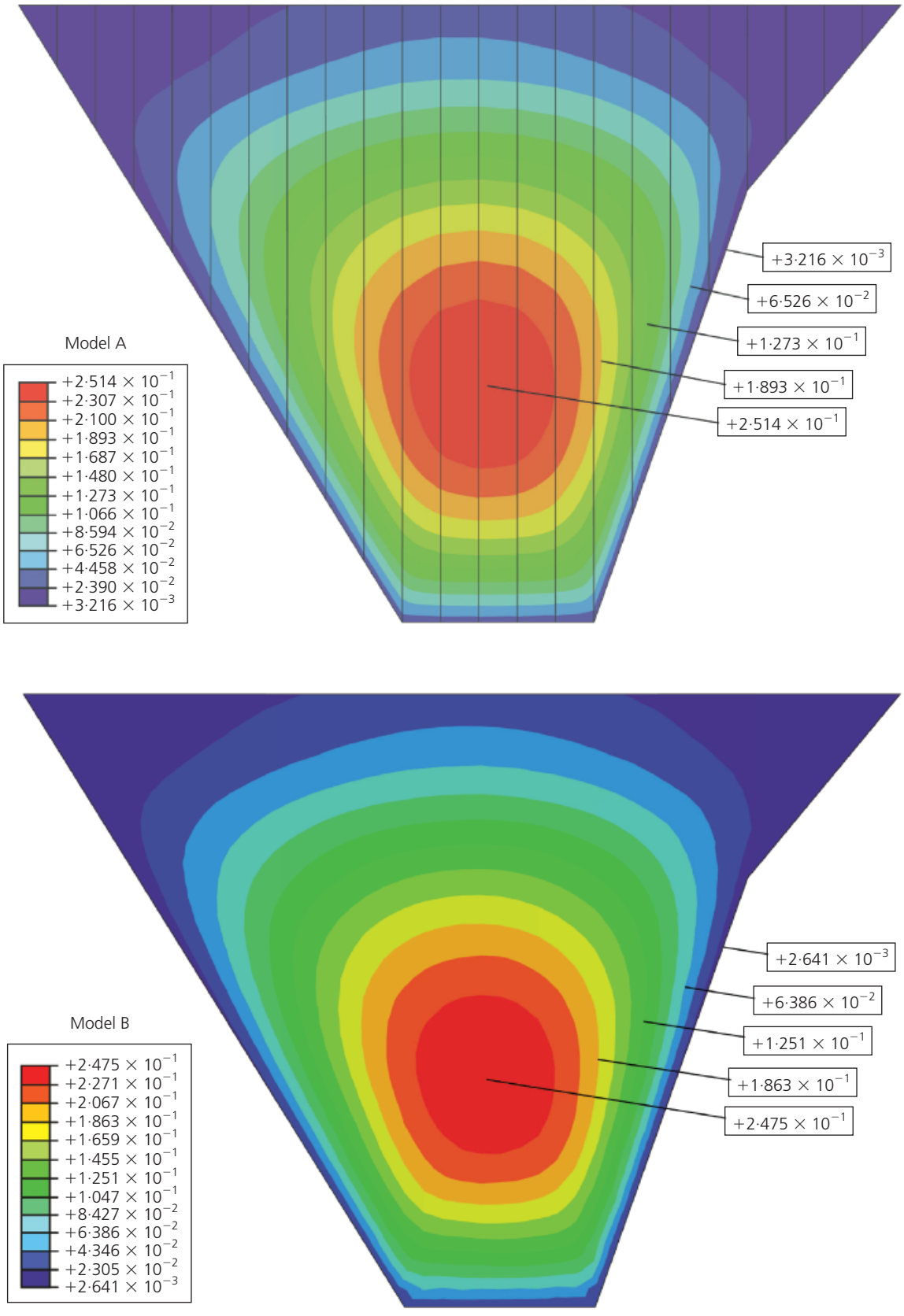

Figure 8. Total deformations of face slabs in models A and B

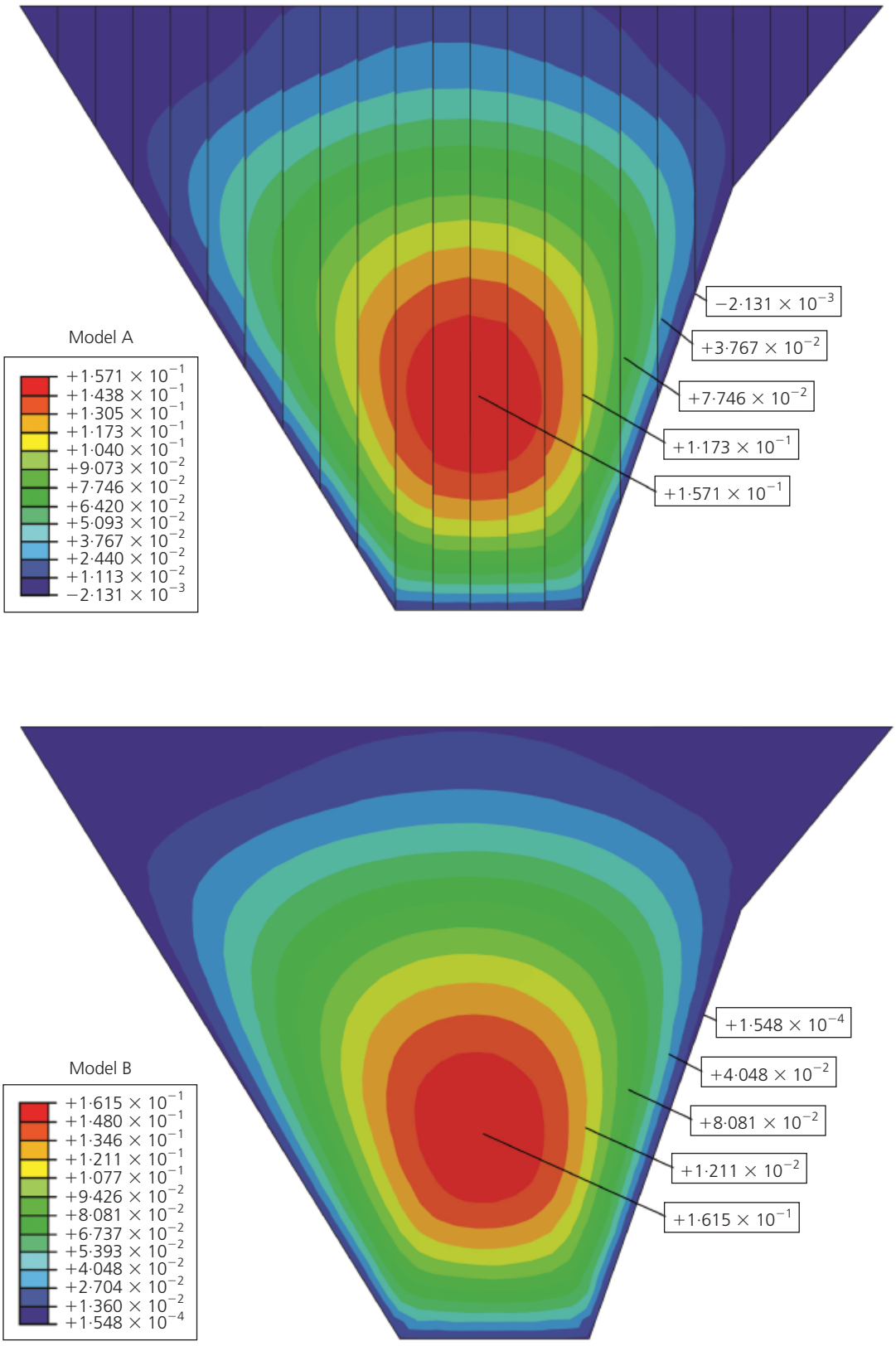

Figure 9. Horizontal deformations perpendicular to dam axis for face slab models A and B

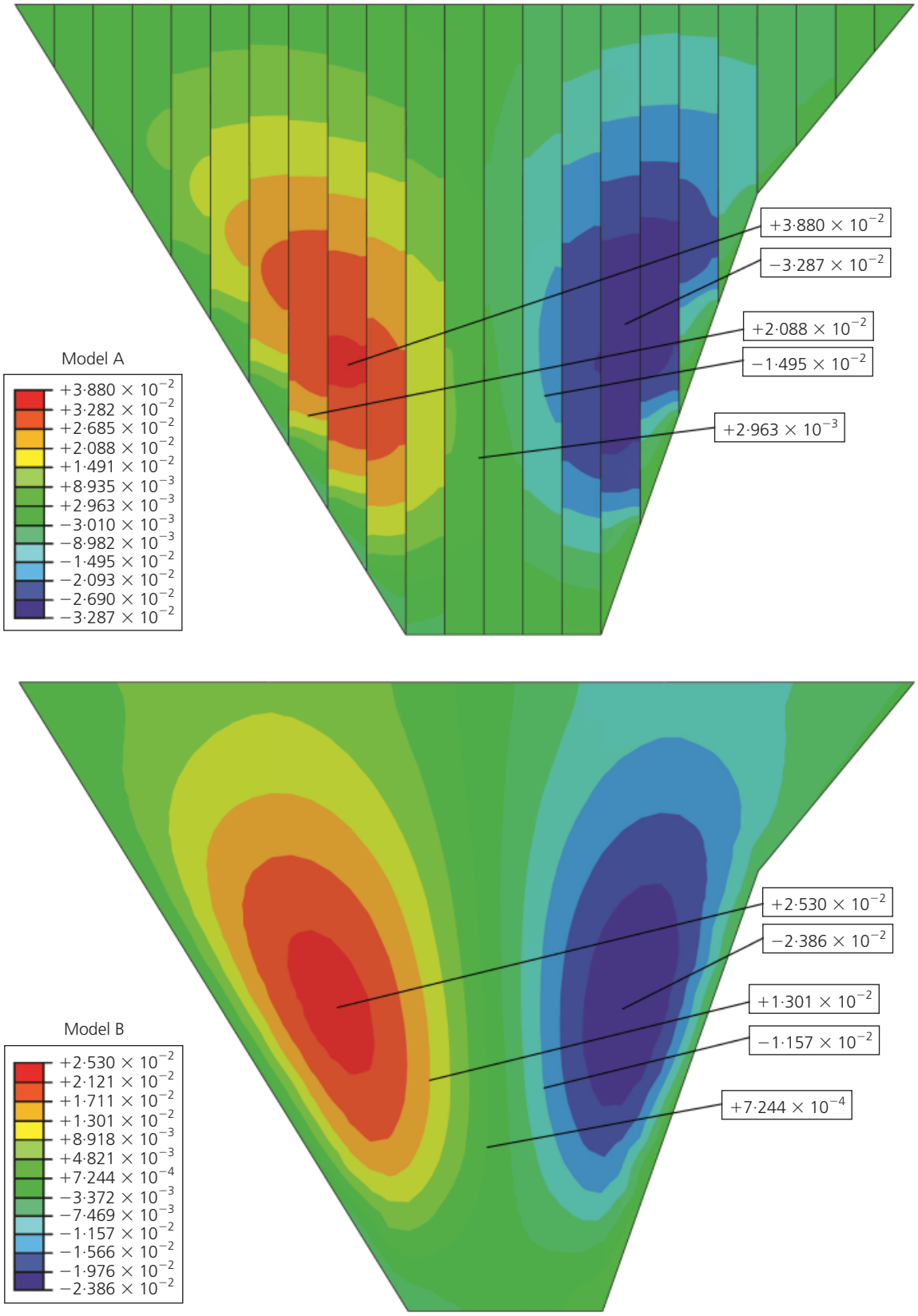

Figure 10. Horizontal in-plane deformations of face slab in models A and B

in which D is the maximum deformation of the face slab due to impounding (cm), measured normal to the face slab and occurring at about 40–50% of the dam height. For the Glevard dam we have

$$D = 0{\cdot}14\frac{H^2}{E_v} = 0{\cdot}14 \times \frac{110^2}{100} = 17 \text{ cm}$$

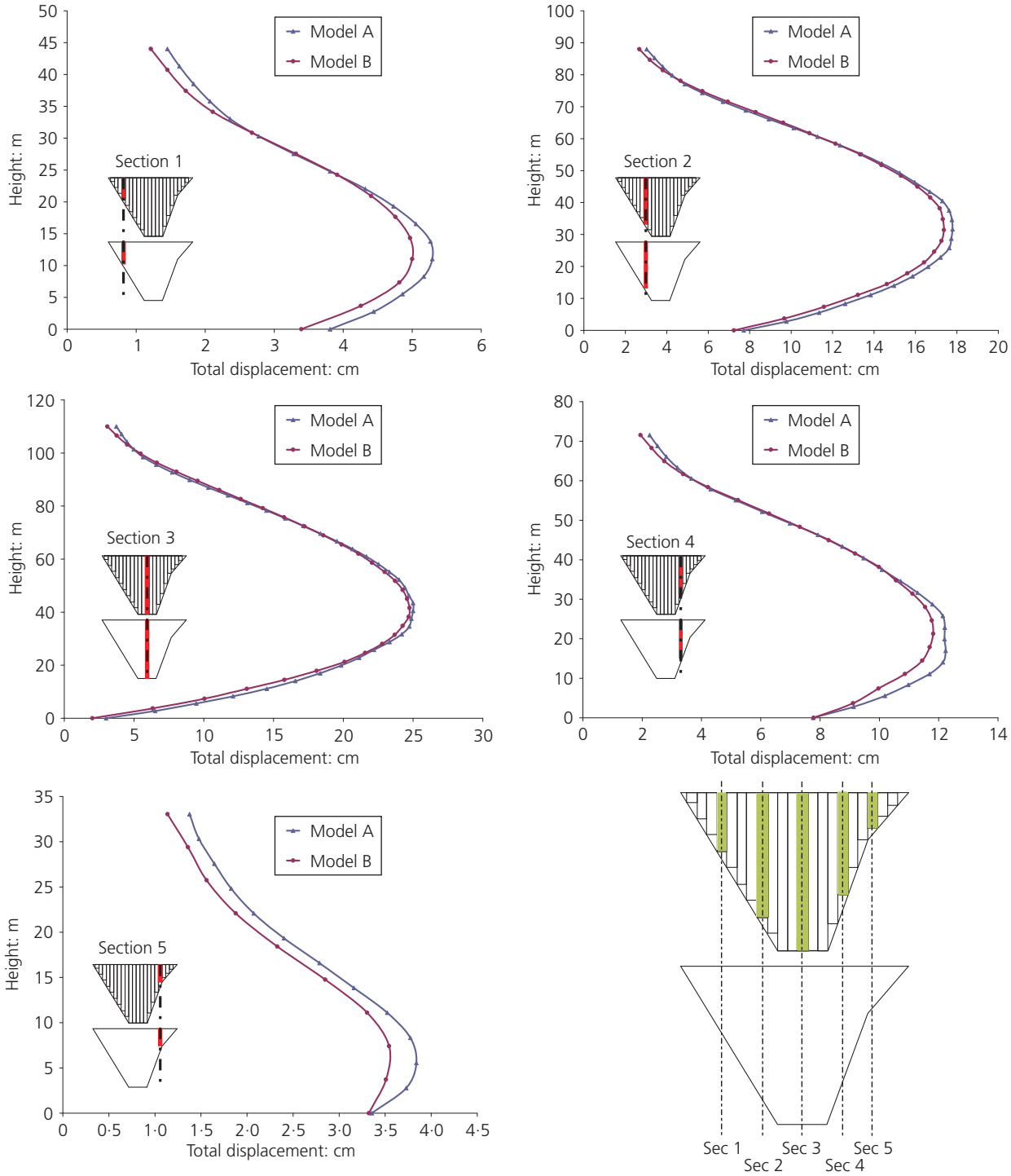

Figure 11. Total deformation of face slab at various sections for models A and B

Based on the results of the 3D FE analysis, the component of the maximum deformation in the direction normal to the face slab is approximately 20 cm, which is reasonably close to the 17 cm estimated above.

Figures 11 and 12 compare variations of the total and horizontal in-plane deformations with elevation respectively, at five selected sections of the Glevard dam face slab. The figures show that whereas deformations are generally higher in model A than in

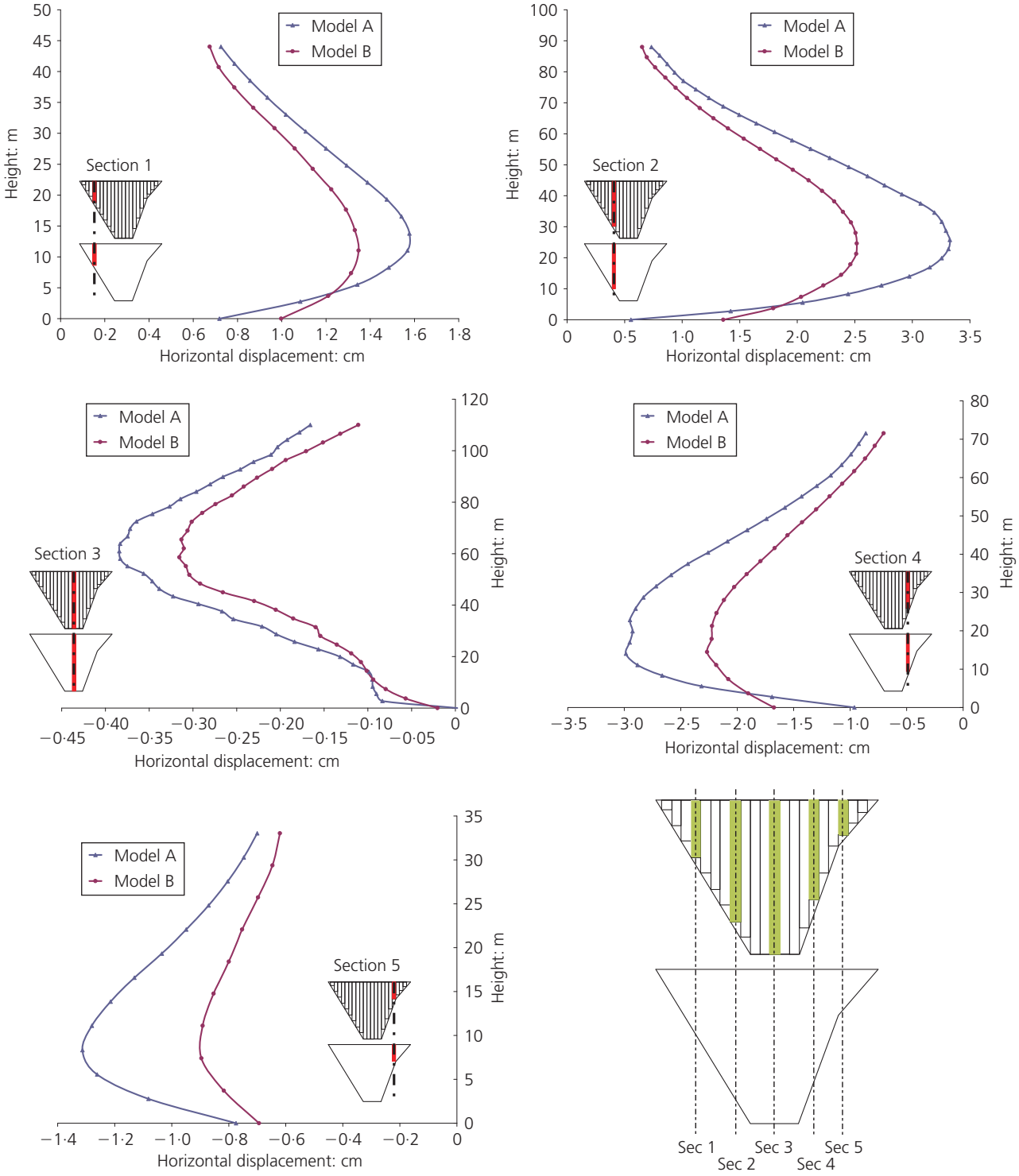

Figure 12. Horizontal in-plane deformation of face slab at various sections for models A and B

model B, the difference is much more pronounced for horizontal in-plane deformations than for the total deformations. However, the horizontal in-plane deformations are not always higher over the whole section height in model A; depending on the valley wall geometry, they are lower than those of model B near the dam foundation in some sections. This might be the result of a more uniform displacement of the whole slab in model B compared with the individual behaviour of each slab section in model A, which depends on the local stress conditions and valley wall geometry. The normal hydrostatic pressure applied to the slab sections is higher at greater depths, resulting in higher shear resistance and smaller deformation or slippage at the slab/upstream slope interface in the taller slab sections in model A.

Figures 11 and 12 also show that whereas the maximum deformation in the middle section (section 3) of the slab occurs at about 40% of the section height above the foundation, which is generally consistent with the observations of Pinto and Marques (1998) described earlier, it occurs closer to the toe of the upstream slope in the shorter sections on the sides of the slab. This is true for both total and horizontal in-plane slab deformations, and might be a result of the smaller height and more translational mode of movements of the shorter, less restricted slab sections on the two sides, compared with the mainly deformational mode of the longer sections that are subject to higher shear resistance against movement at their lower ends near the slope toe, where higher hydrostatic pressures exist.

Figure 11 shows that whereas the maximum total deformations or displacements of the various slab sections vary from approximately 3·8 cm to 25 cm, deformations or displacements of the slab sections at their lower end at the toe of the upstream slope vary over a narrower range of approximately 3·3–7·5 cm. This is approximately true for both models A and B, indicating that the design of the perimeter joint of the face slab may not be significantly affected by the presence or absence of a slab joint.

Table 5 shows that differences in the maximum total deformations of the face slab between models A and B are smaller in the middle sections (e.g. section 3) compared with the side sections (e.g. sections 1 and 5). A similar trend, but with more pronounced differences, is observed in Table 6, in which horizontal in-plane deformations are compared. These results may be attributed to the effects of valley shape and its relative symmetry, differences in the heights of the slab sections in the abutment areas, and the 3D effects of the CFRD behaviour, as discussed before.

Section no.	Slab height: m	Maximum total deformation: cm		
		Model A: cm	Model B: cm	Change from model A to B: %
1	44	5·29	5·00	−5·48
2	88	17·79	17·38	−2·30
3	110	25·00	24·74	−1·04
4	71	12·23	11·82	−3·35
5	33	3·84	3·54	−7·81

Table 5. Difference in total deformations between models A and B

Section no.	Slab height: m	Maximum horizontal in-plane deformation: cm		
		Model A	Model B	Change from model A to B: %
1	44	1·58	1·35	−14·55
2	88	3·32	2·52	−24·09
3	110	−0·38	−0·31	−18·42
4	71	−2·98	−2·27	−23·82
5	33	−1·31	−0·89	−32·06

Table 6. Difference in horizontal in-plane deformations between models A and B

3.3 Face slab joint opening

The importance of appropriate design and construction of joints is easily realised by considering leakage through potential openings at joints or through cracks in face slabs. Leakage is a key indicator of the overall performance of CFRDs. Large leakage rates may indicate that unacceptable openings have occurred at the slab joints, or that the concrete face slab has cracked. Opening of vertical joints may be estimated by the determination of relative movements of points on adjacent slabs. For the face slab in model A, variations and maximum values of openings of vertical joints are presented in Figure 13. As can be seen from this figure, the maximum calculated value of joint opening is about 14 mm, and it occurs at the seventh joint (J 7) located on the valley slope. A review of the data on measured joint openings of CFRDs shown in Table 1 indicates that the calculated maximum joint opening for the Glevard dam is generally consistent with the values measured in similar, previously constructed CFRDs. Figure 13 also shows that the greatest openings occur in joints between slab sections ending on the valley slopes, and the maximum openings occur closer to the toe of the upstream slopes. This is consistent with the trend observed in Figure 12 for the horizontal in-plane deformations of the slab sections, discussed previously. For the Glevard dam, the joint filler and water stop capacity for movement is about 100 mm. Therefore the joint openings obtained from analysis do not exceed tolerable values, and are not expected to lead to leakage through slab joints.

3.4 Face slab stresses

Figures 14 and 15 show the maximum and minimum principal stresses respectively, as obtained from the FE analyses of models A and B. In both models, stresses developed in the central parts of the face slab are compressive (negative), as demonstrated by the negative values of the contours of minimum principal stresses (Figure 15) and the near-zero values of the contours of maximum principal stresses (Figure 14) in these areas. The opposite is observed in the perimeter areas in the lower edges of the slabs near the toe of the upstream slope, where the highest tensile stresses have developed. These results are consistent with the observations of Giudici *et al.* (2000), who indicated that, owing to the load of impounding, the face slab remains in compression over most of its area, but in extension near the dam abutments.

The stress contours indicate that the tensile stresses developed at the perimeter areas of the slabs in both models A and B generally increase with depth, so that their values are highest near the dam foundation and lower at the shallower abutment areas. The development of tensile stresses at the slab edges and their increase with depth are consistent with the increase in the shear resistance at the slab/upstream slope interface. As discussed above, this increase in the shear resistance results from the increase in the normal stresses caused by the hydrostatic pressure at greater depths.

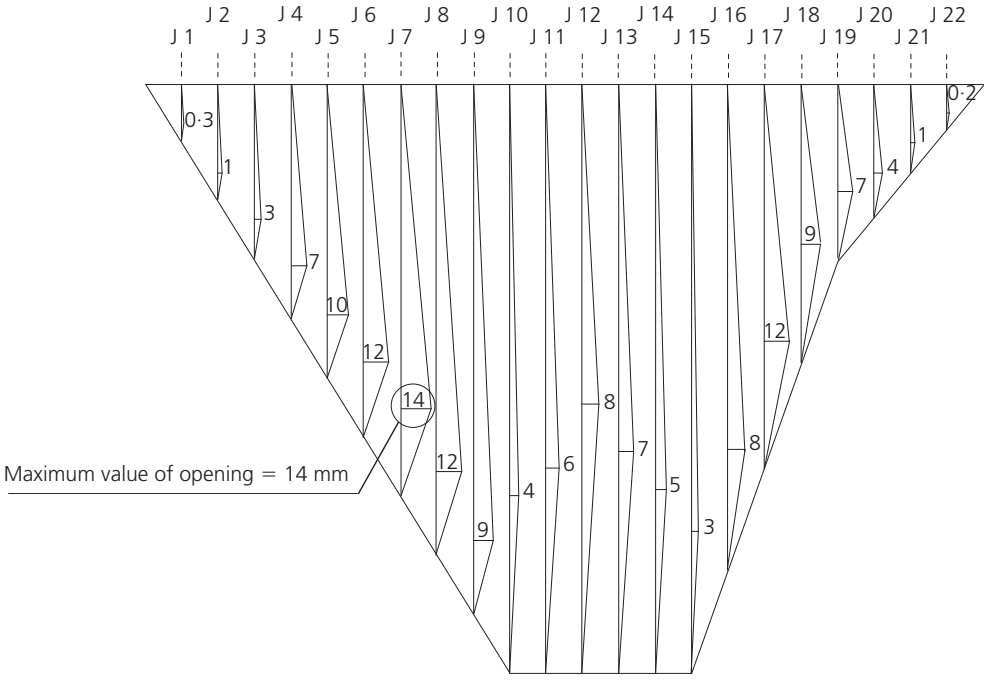

Figure 13. Calculated openings of face slab joints due to impounding (mm)

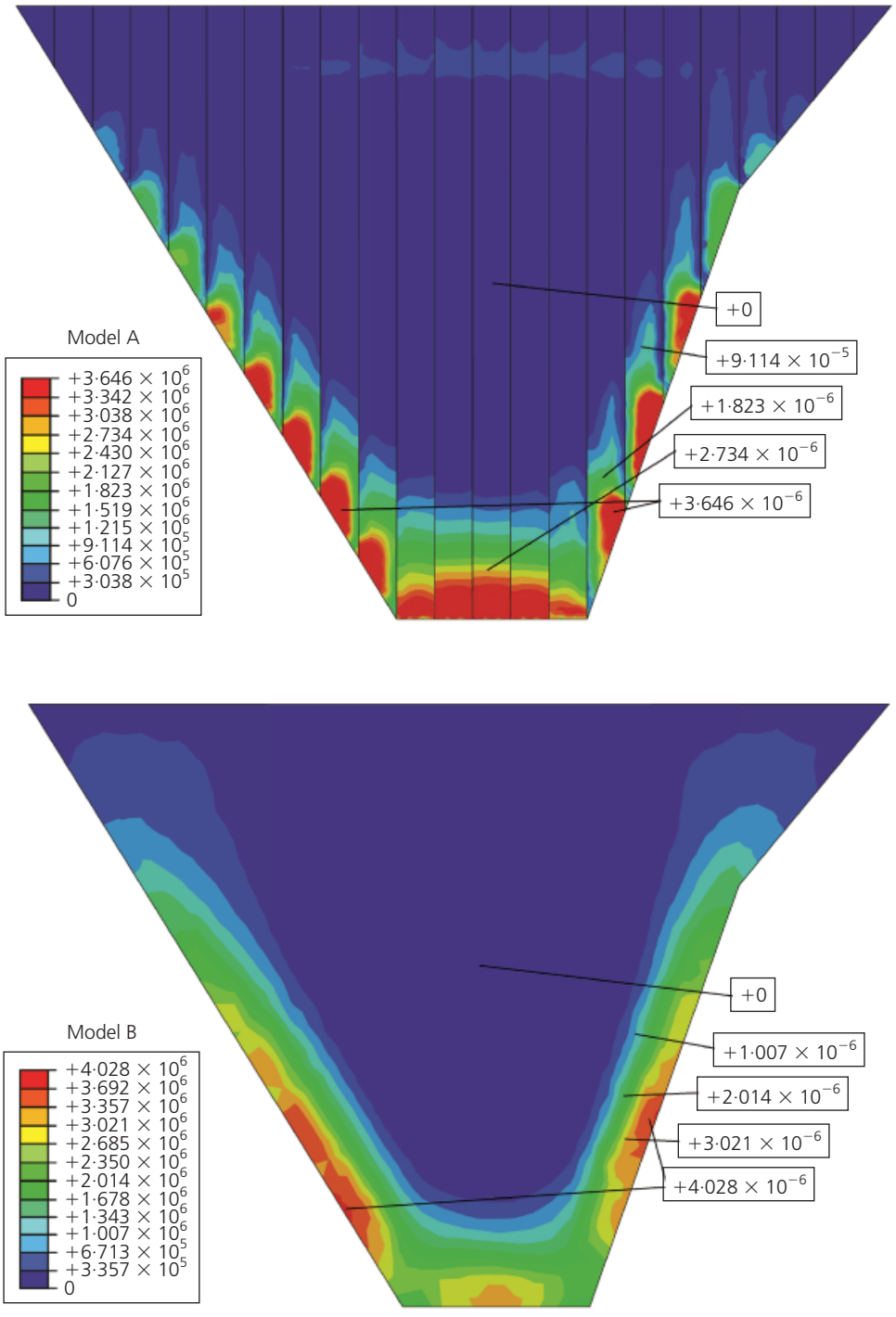

Figure 14. Comparison between maximum principal stresses of face slab for models A and B

3.5 Axial forces in the face slab

Axial force is an important parameter used in the design of face slabs of CFRDs (Uddin, 1999). Figure 16 shows contours of axial forces, and Figure 17 shows a comparison between variations of axial forces with depth at the selected sections from models A and B. The maximum tensile and compressive axial forces obtained at various sections are presented in Tables 7 and 8 respectively, together with comparisons between the results obtained for models A and B. Whereas the highest tensile stress developed in the middle section of the slab is about 14% smaller

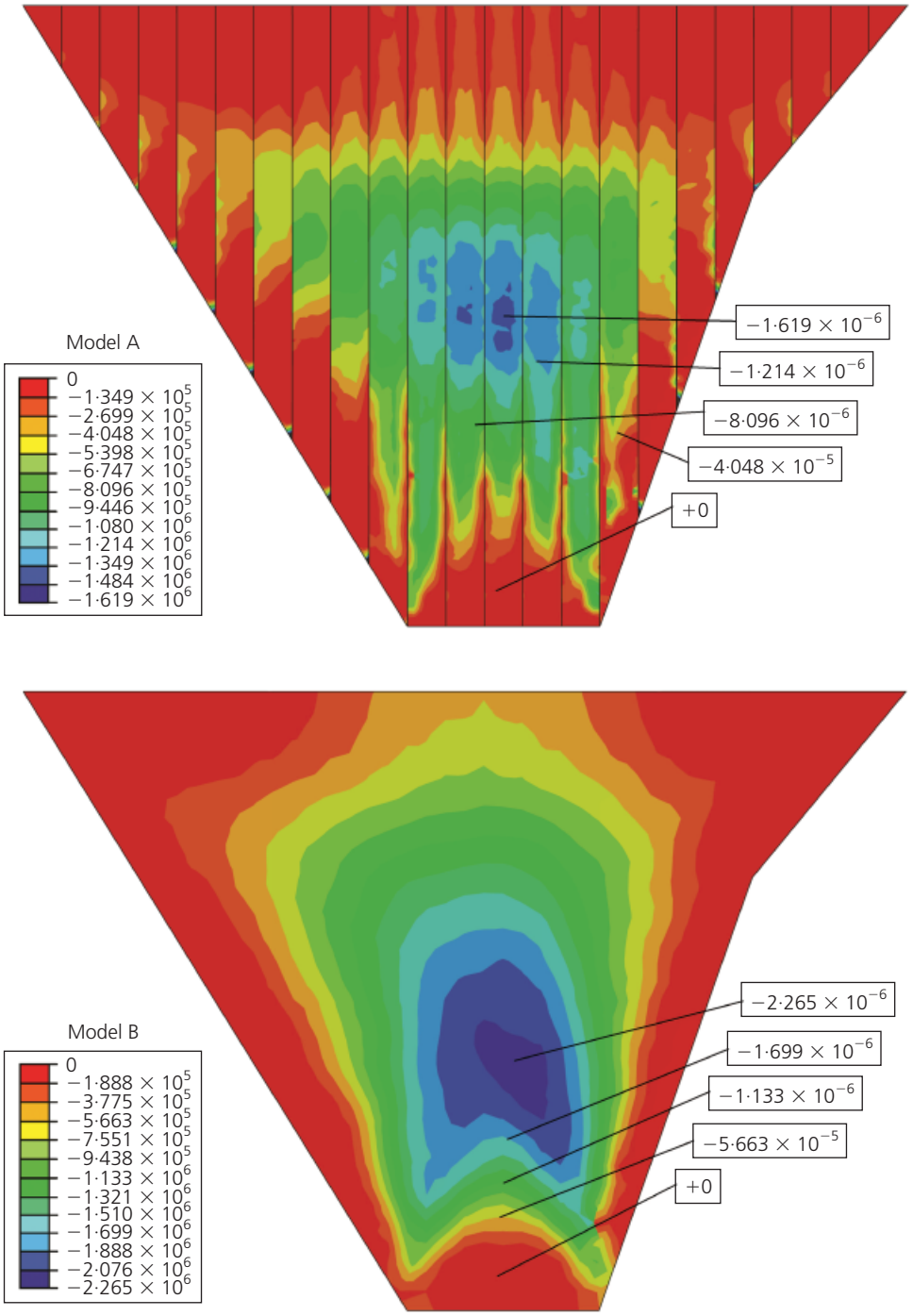

Figure 15. Comparison between minimum principal stresses of face slab for models A and B

in model B (Table 7), the compressive stress calculated in this section is about 6% higher in this model (Table 8). The smaller stresses obtained for the sections on the two sides of the middle section have a generally opposite trend, such that in most of them the tensile stresses increase but the compressive stresses decrease in model B compared with A. Figure 17 shows that the overall difference in the variation of stresses with depth between models A and B is very small at the middle (highest) section, but it generally increases with the increase in distance from the middle section.

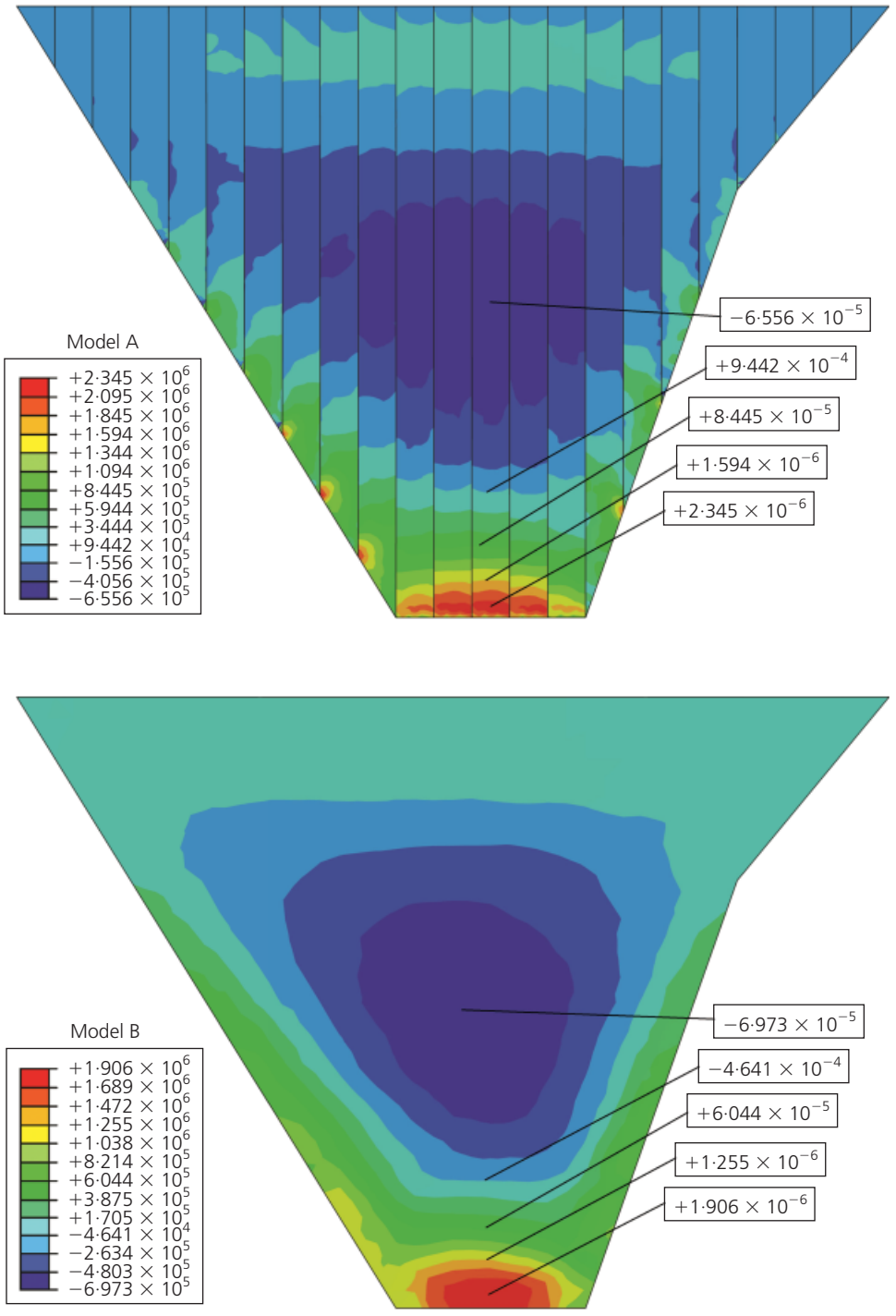

Figure 16. Contours of axial forces developed in face slab in models A and B

4. Summary and conclusions

The behaviour of a 110 m high CFRD and its concrete face slab is examined using the results of 3D FE modelling. Results of the analysis of the dam, which is currently under construction, are verified by comparing them with those obtained from empirical relationships derived from the measured behaviour of other CFRDs, and with databases of measurements on similar dams. Two models were used for the concrete face slab: model A with

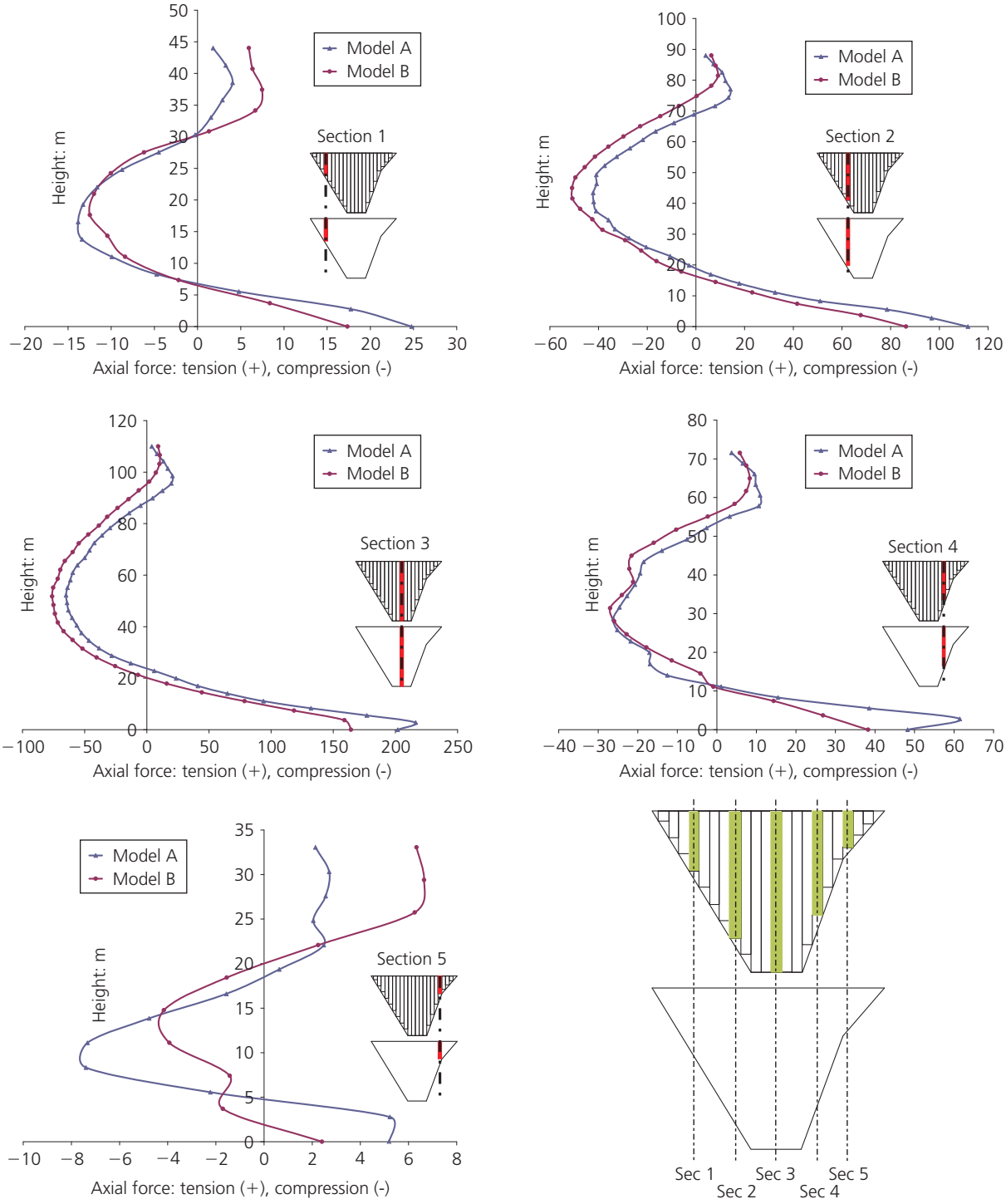

Figure 17. Comparison between calculated axial forces in face slab for models A and B

vertical joints and model B without them. Some results of this study are summarised below.

(*a*) The 3D FE analysis, assuming linear elastic material properties, resulted in a maximum deformation of the face slab, separation in slab joints and construction settlements in reasonable agreement with values obtained from empirical relationships and databases of observed behaviour of other CFRDs.

(*b*) As expected, the face slab with vertical joints behaves more

Section no.	Slab height: m	Maximum tensile axial force: t		
		Model A	Model B	Change from model A to B: %
1	44	24·78	25·44	+2·66
2	88	111·75	97·9	−12·39
3	110	216·31	184·75	−14·59
4	71	61·44	46·1	−24·97
5	33	5·22	7·57	+45·02

Table 7. Comparison between tensile axial forces in face slab for models A and B

Section no.	Slab height: m	Maximum compressive axial force: t		
		Model A	Model B	Change from model A to B: %
1	44	13·83	7·44	−46·20
2	88	42·23	44·5	+5·38
3	110	64·94	69·21	+6·58
4	71	26·2	21·53	−17·82
5	33	7·39	0·92	−87·55

Table 8. Comparison between compressive axial forces in face slab for models A and B

flexibly than that without joints. The difference between the deformations in models A and B is smaller near the middle section of the face slab than in the sections on the two sides. Neglecting the face slab joints in the analysis did not significantly influence the calculated total slab deformations, but it resulted in considerable underestimation of the in-plane horizontal deformations, and an underestimation of some of the axial forces developed in the face slab, especially at the shorter sections near the dam abutments.

(*c*) The calculated horizontal, in-plane displacements of the face slab were substantially smaller than the horizontal displacements perpendicular to the dam axis; however, they can have a greater influence on the openings between the slabs in model A, on the performance of the water stops, and on the potential seepage at the slab joints. The greatest openings were obtained between the slab sections on the two sides, close to the toe of the upstream slope. For the Glevard dam, the joint filler and water stop capacity for movement is about 100 mm, and the 14 mm maximum joint opening obtained from the analysis does not exceed allowable values.

(*d*) Contours of stresses developed in the face slab indicate that, owing to the load of impounding, most of the slab area remains in compression, but tensile stresses also develop at the perimeter areas in both models A and B. Tensile stresses generally increase with depth, and are highest at, or near, the dam foundation. The results showed that the difference in the variation of stresses and axial forces with depth between models A and B is small at the middle (highest) slab section, but it generally increases with distance from the middle section.

(*e*) The normal hydrostatic pressure applied to the slab is higher at greater depths, resulting in higher shear resistance at the interface between the slab and the upstream slope. This might be responsible for the smaller deformation of the lower end (near the toe of the upstream slope) of the middle section compared with the side sections, the smaller deformation of the lower end of the slabs in model A compared with B, and the higher tensile stresses developed in the slabs at greater depths.

REFERENCES

Ev Yol–Ab Niru (2010a) *2D/3D Static and Dynamic Analyses of Rockfill and Concrete Face Slab for Different Loading Conditions*. Ev Yol–Ab Niru Group Co., Tehran, Iran, Report No. 1.2.2.

Ev Yol–Ab Niru (2010b) *Summary of Static and Dynamic Analyses of the Glevard-Neka Dam*. Ev Yol–Ab Niru Group Co., Tehran, Iran (in Farsi).

Giesecke J, Rommel M and Soyeaux R (1991) Seepage flow under

dams with jointed rock foundation. *Proceedings of the 17th Congress on Large Dams, Vienna, Austria*.

Giudici S, Herweynen R and Quinlan P (2000) HEC experience in concrete faced rockfill dams, past, present and future. *Proceedings of the International Symposium on Concrete Faced Rockfill Dams, Beijing, China*, pp. 29–46.

Hunter G, Glastonbury J, Ang D and Fell R (2003) *The Performance of Concrete Face Rockfill Dams*. The University of New South Wales, Sydney, Australia.

ICOLD (2004) *Concrete Face Rockfill Dams: Concepts for Design and Construction*. 2004. International Commission on Large Dams, Paris, France.

Kashiwayanagi M, Koizumi S, Ishimura Y and Kakiage HA (2000) Fundamental study on the face slab joint behaviour of the CFRD. *Proceedings of the International Symposium on Concrete Faced Rockfill Dams, Beijing, China*, pp. 341–349.

Marulanda C and Anthiniac P (2009) Analysis of a concrete faced rockfill dam including concrete face loading and deformation. *Proceedings of the 10th Benchmark Workshop on Numerical Analysis of Dams, Paris, France*.

Noorzaei J and Mohammadian E (2000) Modeling of concrete face rockfill dam via finite-infinite and interface elements. *Proceedings of International Symposium on Concrete Faced Rockfill Dams, Beijing, China*, pp. 361–70.

Pinto NLS and Marques FP (1998) Estimating the maximum face deflection in CFRDs. *International Journal on Hydropower and Dams* **5(6)**: 28–31.

Swaisgood JR (1995) Estimating deformation of embankment dams caused by earthquakes. *Association of State Dam Safety Officials, Western Regional Conference, Red Lodge, MT, USA*, pp. 1–7.

Uddin N (1999) A dynamic analysis procedure for concrete-faced rockfill dams subjected to strong seismic excitation. *Computers and Structures* **72(1–3)**: 409–421.